General Disclaimer

One or more of the Following Statements may affect this Document

- This document has been reproduced from the best copy furnished by the organizational source. It is being released in the interest of making available as much information as possible.

- This document may contain data, which exceeds the sheet parameters. It was furnished in this condition by the organizational source and is the best copy available.

- This document may contain tone-on-tone or color graphs, charts and/or pictures, which have been reproduced in black and white.

- This document is paginated as submitted by the original source.

- Portions of this document are not fully legible due to the historical nature of some of the material. However, it is the best reproduction available from the original submission.

INVESTIGATION OF THE OXIDATION BEHAVIOR OF DISPERSION STABILIZED ALLOYS WHEN EXPOSED TO A DYNAMIC HIGH TEMPERATURE ENVIRONMENT

Final Report

Metallurgical Engineering
Division of Minerals Engineering

NASA Grant NGR-47-004-082

D. R. Tenney
Principal Investigator

INTRODUCTION

The oxidation behavior of TD-NiCr and TD-NiCrAlY alloys have been studied at 2000° and 2200°F in static and high speed flowing air environments. The TD-NiCrAlY alloy preoxidized to produce an Al_2O_3 scale on the surface showed good oxidation resistance in both types of environments. The TD-NiCr alloy which had a Cr_2O_3 oxide scale after preoxidation was found to oxidize more than an order of magnitude faster under the dynamic test conditions than at comparable static test conditions. Although Cr_2O_3 normally provides good oxidation protection, it was rapidly lost due to formation of volatile CrO_3 when exposed to the high speed air stream. The preferred oxide arrangement for the dynamic test consisted of an external layer of NiO with a porous "mushroom" type morphology, an intermediate duplex layer of NiO and Cr_2O_3, and a continuous inner layer of Cr_2O_3 in contact with the alloy substrate. An oxidation model has been developed to explain the observed microstructure and overall oxidation behavior of the alloys.

To fully document the results of this research effort, three journal articles have been written. Copies of these articles have been included to give a summary of the important experimental findings of the work performed under this grant. The titles of these articles are as follows:

1. "Oxidation Behavior of TD-NiCr in a Dynamic High Temperature Environment", Met. Trans., 5, 1001-11 (1974), by D. R. Tenney, C. T. Young, and H. W. Herring.
2. "Interdiffusion in the Ni/TD-NiCr and Cr/TD-NiCr Systems," Met. Trans., 5, (1974), by A. V. Pawar and D. R. Tenney.
3. "Dynamic Oxidation Behavior of TD-NiCr Alloy with Different Surface Pretreatments", Met. Trans, 5, (1974), by C. T. Young, D. R. Tenney, and H. W. Herring.

A fourth paper is currently under preparation and will be submitted for publication in the near future. A draft of that paper will be forwarded to the technical monitor of this grant at the same time it is submitted for journal publication.

In addition to the papers written on the work performed under this grant, a number of technical talks have been presented at national meetings. The titles of these talks along with the location and data presented are given below:

1. "High Temperature Oxidation of TD-NiCr and TD-NiCrAlY in a Flowing Air Environment", 77th National Meeting, American Institute of Chemical Engineers, Pittsburg, Pa., June 25, 1974.
2. "The Dynamic Oxidation Behavior of TD-NiCr", (with C. T. Young and H. W. Herring), Annual Fall Meeting of Metallurgical Society of AIME, Chicago, Ill., Oct. 1-4, 1973.
3. "Oxidation Behavior of TD-NiCr in a Dynamic High Temperature Environment", (with C. T. Young and H. W. Herring), Annual Spring Meeting of Metallurgical Society of AIME, Philadelphia, Pa., May 29-June 1, 1973.
4. "Effect of Surface Pretreatment on the Static and Dynamic Oxidation Behavior of TD-NiCr", (with C. T. Young), Annual Meeting of the Virginia Academy of Science, Williamsburg, Va., May 5, 1973.
5. "An Analytical Model for the High Temperature Oxidation of Thoria Dispersed Nickel Chromium Alloy", (with A. V. Pawar), Annual Meeting of the Virginia Academy of Science, Williamsburg, Va., May 5, 1973.
6. "Oxidation Behavior of TD-NiCr in a Dynamic High Temperature Environment", (with C. T. Young), Annual Meeting of the Virginia Academy of Science in Lexington, Va., May 5, 1972.

7. "Mathematical Model of the High Temperature Oxidation of TD-NiCr", (with A. V. Pawar), Annual Meeting of the Virginia Academy of Science in Lexington, Va., May 5, 1972.

NASA support of this research effort has been greatly acknowledged in all talks presented and papers published.

DYNAMIC OXIDATION BEHAVIOR OF TD-NiCr ALLOY WITH DIFFERENT SURFACE PRETREATMENTS

C. T. Young and D. R. Tenney
Metallurgical Engineering Department
Virginia Polytechnic Institute and State University
Blacksburg, Virginia 24061

H. W. Herring
NASA Langley Research Center
Hampton, Virginia 23365

ABSTRACT

Oxidation tests of TD-NiCr alloy with different surface pretreatments were conducted in a Mach-5 arc-jet at 1200°C and 0.002 lb/sec. flowing air environment. Extensive scanning electron microscopy and X-ray analyses were carried out to determine the mechanisms responsible for the observed oxidation behavior. The presence of atomic oxygen in the air stream plays a significant role in determining the oxidation behavior of the alloy. The rate of Cr_2O_3 vaporization by formation of volatile CrO_3 is greatly enhanced by the flowing conditions. The typical microstructure of oxides formed in the dynamic tests consists of an external layer of NiO with a porous "mushroom" type morphology, an intermediate layer of NiO and Cr_2O_3 oxide mixture, and a continuous inner layer of Cr_2O_3 in contact with the Cr-depleted alloy substrate. The formation of mushroom type NiO is attributed to three basic processes: (1) vaporization of NiO by dissociation into its elements, (2) reoxidation of Ni vapor predominantly with atomic oxygen, and (3) condensation of NiO at elevated sites on specimen surface. The rate of oxidation is controlled by an interplay between the rate of loss of NiO in the vaporization-condensation process and the rate of growth of the inner

Cr_2O_3 layer. Surface preparation has a significant influence on the morphology, order and relative amount of NiO and Cr_2O_3 formed during the initial stages of oxidation, but becomes less important as exposure time increased. The observed oxidation behaviors can be explained in terms of a general model encompassing the basic oxidation and vaporization-condensation processes.

INTRODUCTION

Ni-20%Cr-2%ThO_2 alloy supplied under the trade name of TD-NiCr has been considered for use in advanced jet engines and as a part of thermal protection system for space shuttle because of its reported high strength and good static oxidation resistance at high temperature[1-10]. The addition of submicron ThO_2 particles to the Ni-Cr alloy inhibits grain growth and stabilizes the substructure of the alloy thereby retaining high strength at elevated temperature[2-4]. The addition of thoria particles also improves static oxidation resistance by promoting the selective oxidation of Cr to form protective Cr_2O_3, and by decreasing the growth rate of Cr_2O_3[6-9]. Surface preparation has a significant influence on the oxidation behavior of the alloy. Surface grinding enhances the formation of Cr_2O_3 whereas electropolishing promotes the formation of external NiO and inner Cr_2O_3 subscale[8-12].

Under high temperature high speed flowing gas conditions a substantial increase in the oxidation rate has been observed as compared with the results of static testing. Gilbreath[13,14] has emphasized the importance of atomic oxygen which existed in the re-entry environment, and has demonstrated the accelerated degradation of the alloy in dissociated oxygen. The result of Lowell et al[15] indicated that the loss rate of material in a 1-atmosphere, Mach-1 turbine gas stream at 1200°C was about 100 times greater than that of static tests. Enhanced oxidation in Mach-1 burner gas stream at 2000°F was also observed by Johnston et al[16]. Centolenzi et al[17,18] have reported the increased oxidation in a Mach-5 arc-jet gas stream, but no detailed mechanism has been given.

In a preceeding paper[19] the oxidation behavior of TD-NiCr (belt-sanded surface finishing) in a Mach-5 arc-jet at 1200°C was reported. It was demonstrated that the external Cr_2O_3 formed during a static preoxidation was not stable in the high speed gas flow and was rapidly replaced by a layer of NiO with a porous "mushroom" type morphology. In that work metal recession was measured. It was found that the substrate thickness decreased rapidly at the early stages of oxidation, and decreased linearly with time at a much slower rate in the later stages of oxidation. A model was proposed to explain the observed oxidation behavior. To further confirm the proposed model, a comprehensive metallographic analysis of the oxidation behavior of specimens having four different surface pretreatments was investigated in the present study. Oxidation tests were conducted with emphasis being placed on short time tests where the effect of the original surface condition should be most important. The chronology of oxidation for each surface preparation and test time was fully documented. The data thus collected was combined with that reported earlier to provide a better characterization of the oxidation behavior of TD-NiCr under simulated shuttle re-entry conditions.

Experimental Procedures

The TD-NiCr specimens used in this study were prepared from the same 0.02 inch thick sheet stock as those reported in the previous paper[19]. The sheet stock was received in a recrystallized condition with a belt-sanded surface finish. Specimen configuration and alloy microstructure have been described in the same previous paper. To reveal the effect of surface pretreatment on the oxidation behavior, specimens were given four

different surface treatments prior to dynamic oxidation tests. The four surface preparations added to the as-received specimens were: (1) electropolishing, (2) mechanical polishing, (3) electropolishing followed by static preoxidation, and (4) mechanical polishing followed by static preoxidation. In this paper they will be abbreviated as (1) EP, (2) MP, (3) EP + PO, and (4) MP + PO, respectively. Mechanical polishing was finished through 600 grit SiC abrasive paper. Electropolishing was carried out in a solution of 87 ml methanol, 8 ml H_2SO_4, 3 ml HNO_3 and 2 ml HF at room temperature and 17 volts for 2 minutes. The static preoxidation was conducted in air at 1100°C for one hour. The purpose of this preoxidation was to produce different surface oxides as starting conditions of dynamic tests.

The dynamic oxidation tests were conducted in a Mach-5 arc-jet operated with a mass flow of 0.002 lbs/sec. air. Details on the arc-heater equipment have been described in the previous paper[19]. The power to the arc-heater was adjusted to yield a gas temperature sufficient to maintain a specimen test temperature of 1200°C under lamellar flow conditions. In general it was found necessary to use lower initial power for the un-preoxidized specimens, especially those electropolished, than for those which had been preoxidized. During the initial few minutes of testing it was necessary to continually increase the power to maintain a constant test temperature. Once the metallic surfaces were covered with stable oxide scales with essentially the same surface reflectance and emittance the power approached to a value common to all the tests. Specimens were oxidized in the arc-heater for times ranging from 12 seconds to 10 hours. All tests for times longer than 30 minutes were cyclic tests of 30 minutes duration followed by cooling before

the next run. This procedure was repeated until the desired cumulative exposure time was obtained.

The oxide phases present on the oxidized specimens were identified, in situ, using standard X-ray diffraction techniques. Oxide morphology was examined in a scanning electron microscope. Specimens were then sectioned, epoxy mounted, metallographically polished, and vapor deposited with a thin layer of carbon. The microstructure of the oxide cross-sections was analyzed using a scanning electron microscope equipped with an energy dispersive X-ray analyzer (EDAX). Electron probe microanalysis was carried out using an ARL electron microprobe operated at 15 KV and 0.05 μ amp. beam current. The carbon layer deposited on the specimen surface was found to help eliminate shifting of the electron beam at the metal/oxide interface. MAGIC computer program developed by Colby[20] was used to correct the raw data.

Experimental Results

The oxides produced on the tested specimens were identified in situ by X-ray diffraction. The reflections from the alloy and oxide phases detected after each exposure time for the four different types of specimens are listed in Table I. It should be pointed out that the as-recieved alloy sheet had a very strong preferred orientation with {100} planes parallel to the specimen surface. No {111} reflection was observed from the as-received specimens. The {111} alloy reflection was, however, always found from the mechanically polished specimens after testing or after static preoxidation The presence of this {111} reflection can be taken as direct confirmation of surface recrystallization. For static oxidation it is well known that the effect of this recrystallization is to promote the selective oxidation of Cr_2O_3 [12]. Its effect on the dynamic oxidation behavior of this alloy will be discussed later in this paper.

In the following sections each type of surface pretreatment will be treated separately. Scanning electron micrographs showing the surface morphology and oxide cross-section, energy dispersive X-ray analysis (EDAX) patterns indicating oxide chemistry, and electron microprobe scans showing composition profiles are presented sequentially according to the surface pretreatment.

Electropolished and Preoxidized Surface Finish (EP + PO)

The oxides formed on the electropolished specimen during one hour static oxidation in air at 1100°C consists of an external layer of NiO, a continuous inner layer of Cr_2O_3, and an intermediate layer which is a mixture of NiO and Cr_2O_3. This can be seen in Figure 1, where the oxidized specimen surface, oxide cross-section, and three EDAX patterns taken from different

oxide layers are given. Multiple oxide layers are clearly visible in Figure 1(b). The faceted and granular external oxide, shown in Figure 1(a), is identified to be NiO from the EDAX pattern of spot-3. The absence of a thorium peak in the EDAX pattern indicates that the NiO grew externally by outward diffusion of Ni^{++} ions which reacted with oxygen at the gas/oxide interface. The oxide grains grew predominantly along certain crystallographic directions, thus resulting in a faceted appearance with sharp grain ridges and valleys. The intermediate layer which appears to be porous and grainy is composed of Cr_2O_3 and NiO. The fact that a thorium peak is detected in the corresponding EDAX pattern (spot-2 pattern) suggests that this oxide layer is produced by internal oxidation. Solid state reaction between NiO and Cr_2O_3 might occur to form $NiCr_2O_4$. However, no spinel peaks were ever detected in the X-ray diffraction analysis. Partial dissociation of NiO must have taken place in this duplex oxide layer to provide for Ni^{++} and O^{--} ions required for the observed external growth of NiO and the internal oxidation of the alloy. Counter to the flow of Ni^{++} ions there was inward diffusion of vacancies. Formation of voids at this duplex oxide layer as a result of vacancy condensation weakened the oxide adherence, and is believed to be responsible for the occational spalling of the external NiO layer. The continuous inner oxide layer adjacent to the alloy is Cr_2O_3 (spot-1 EDAX pattern). Although multiple oxide layers were present on the specimen, only NiO was detected in X-ray diffraction studies (Table I). Absorption of the incident and diffracted X-ray beams by the external NiO reduced the intensity diffracted by the inner Cr_2O_3 below the minimum detectable level. Low magnification micrographs taken of specimen surfaces clearly showed the alloy grain structure. Selective oxidation of Cr along alloy grain boundaries greatly reduced the local external growth rate of NiO causing valleys to appear on the surface along the original alloy grain boundaries.

In the previous studies[19], the stable external oxide observed on specimens after dynamic testing was a layer of porous NiO. As noted above, the external oxide on the EP + PO specimens was a layer of solid NiO. For this reason, the dynamic oxidation behavior of EP + PO specimens was studied in detail with emphasis placed on short time tests. The objective was to characterize the development of a stable oxide under the high temperature flowing air conditions. The surface oxide morphologies formed on specimens after 12 and 15 seconds of exposure are illustrated in Figure 2. It should be pointed out here that the time required to heat a specimen in the arc heater to the test temperature was approximately 10 to 12 seconds, according to measurements made using an optical pyrometer and using a thermocouple attached to the back of the specimen. The micrographs in Figure 2 disclose that the faceted NiO which is stable in static oxidation degrades rapidly upon exposure to the dynamic enviornment. At 12 seconds of exposure, Figure 2(a), voids and cracks are seen on the surface mostly along oxide grain boundaries. After 15 seconds of exposure, Figure 2(b) and 2(c), large voids are observed at lower areas of the surface mostly at oxide grain valleys. Some porous mass which is identified as NiO is seen to condense at higher locations on the surface predominantly at oxide grain ridges. Obviously, mass transport from oxide boundary regions to oxide grain ridges has taken place at the specimen surface immediately upon exposure to the high temperature flowing air. Grimley et al.[21] have reported that the vaporization of NiO at high temperature is predominantly by dissociation of NiO into its elements. Equilibrium partial pressures of Ni(v) and O measured on NiO(s) under neutral conditions were reported to be two orders of magnitude greater than that of NiO(v). It will be shown later (Figure 5) that the oxide morphologies illustrated in Figure 2 may be observed only if specimens are tested in a gas stream containing oxygen. It is therefore proposed that the

observed mass transport phenomenon develops following three processes. They are: (1) vaporization of NiO at grain boundary areas mainly by dissociation of NiO into Ni(v) and O, (2) reoxidation of Ni vapor, presumably with atomic oxygen in gas stream, and (3) condensation of NiO at raised points on the surface. The stagnation layer under the present test conditions was reported to be of the order of 360 μm[24]. There are gradients in oxygen concentration and in total pressure across the thickness of the stagnation layer. Vaporization of NiO appears to proceed at a faster rate at areas lower than the average specimen surface level where the total pressure is somewhat lower under the flowing conditions. Consequently, voids and cracks are observed mostly along oxide grain valleys. Reoxidation of Ni vapor tends to take place at a greater rate at locations above the average surface level where the oxygen partial pressure is higher. Therefore, condensation of NiO occurs mostly at higher locations on the specimen surface where the rate of reoxidation of Ni vapor is greater than the rate of loss to the flowing air stream.

During subsequent oxidation the vaporization-condensation process brings about some drastic changes in the oxide morphology. The micrographs shown in Figure 3 were taken of EP + PO specimens which had been oxidized in the arc heater for 1 and 10 minutes, respectively. After one minute of oxidation, the specimen surface is covered with a layer of very porous oxide, see Figure 3(a). High magnification photographs and EDAX patterns reveal that the porous oxide consists of numerous fine NiO crystals, with an appearance similar to that sometimes observed for crystals growing under condensation processes. The oxide cross-section shown in Figure 3(b) strongly suggests that the surface oxide clusters develop by mass transport through the proposed vaporization, oxidation, and condensation processes. The top portion of

the original NiO which formed during static preoxidation degrades as a result of prevailed vaporization. There are fine particles of NiO growing on top of the corroded NiO layer as a consequence of condensation of re-oxidized NiO. The oxides underneath the degraded layer remain essentially uneffected.

After 10 minutes of oxidation, most of the specimen surface is covered with a layer of NiO, the top of which has a "mushroom" type morphology, Figure 3(c). At some other areas, predominantly the areas near alloy grain boundaries, NiO "mushroom" clusters smaller than those shown in the figure were observed. This can be attributed to the fact that the original NiO surface layer was thin at the alloy grain boundary regions because of the preferential formation of Cr_2O_3 during the preoxidation treatment. The microstructure of the oxide cross-section at areas where large "mushrooms" developed is given in Figure 3(d). The NiO clusters consisting of fine NiO particles are supported by oxide stems which are the remains of the original NiO. The mushroom oxide grows at the expense of the original NiO layer. Although part of the NiO condenses on growing mushrooms, a significant fraction of it is carried away by the flowing gas. Most of the original NiO disappears after about 30 minutes of oxidation. From this stage on the existance of mushroom oxide depends on the NiO in the duplex oxide layer. As the NiO content in the duplex oxide layer is low (see spot-2 pattern in Figure 1), the mushroom clusters start to reduce in size because the rate of supply of Ni becomes less than the rate of loss to the gas stream by vaporization.

Micrographs illustrating the topography and structure of oxide formed on an EP + PO specimen after 2 hours of exposure are presented in Figure 4. These micrographs are also typical for specimens after 10 hours of oxidation.

At this later stage of oxidation, most of the specimen surface is covered with small mushroom type oxide clusters. These small clusters exhibit a relatively smooth surface as compared with that of the large mushrooms found in the earlier stages of oxidation. A typical micrograph showing the small mushroom type oxide is given in Figure 4(a). A micrograph revealing the corresponding oxide cross-section is presented in Figure 4(b). Islands of large mushrooms were also observed on the specimen surface. Local oxidation penetration was normally found underneath the areas where the large oxide clusters formed. An example is given in Figure 4(c) in which three oxide layers are distinguishable. At regions, such as the area shown in Figure 4(b), where the oxide mushrooms and oxide mixture have totally evaporated, the inner Cr_2O_3 is subject to rapid vaporization thus exposing the Cr-depleted alloy directly to the atmosphere. Microprobe scans made at such regions always show extensive Cr depletion in the underlying alloy. In most cases the Cr content is reduced to approximately 10-12% at the alloy/oxide interface. When the alloy is exposed directly to the flowing air, rapid internal oxidation takes place with both NiO and Cr_2O_3 forming simultaneously. A large fraction of the Cr-depleted zone is consumed until a continuous Cr_2O_3 inner layer is finally developed at the oxidation front. This inner layer effectively stops the inward growth of the oxide. Figure 4(c) illustrates a typical oxide structure after the formation of the Cr_2O_3 layer. Microprobe scans made at the penetrated regions suggest that there is a critical Cr concentration below which the continuous Cr_2O_3 layer does not form. This critical value appears to be approximately 15%. Results of a probe scan made along the marked line in Figure 4(c) are shown in Figure 4(d). The Cr content at alloy/oxide interface is approximately 15%. The Ni content in the intermediate oxide layer is about twice that of Cr. This, together with the fact

that no $NiCr_2O_4$ reflections could be identified in X-ray analysis, indicates that the intermediate layer is a mixture of Cr_2O_3 and NiO. At the newly oxidized areas, the NiO supply in the oxide mixture is replenished, and the overlaid mushroom clusters will increase in size until this supply runs low.

From the above observations, it is postulated that for the later stages the oxidation behavior of TD-NiCr alloy can be characterized by local oxidation which proceeds through the cyclic processes of (1) rapid oxidation of unprotected Cr-depleted alloy until a Cr_2O_3 inner layer forms, (2) external growth of NiO mushrooms by vaporization-condensation process at the expense of NiO in the duplex oxide layer, and concurrent vaporization of Cr_2O_3 in the oxide mixture, and (3) rapid vaporization of inner Cr_2O_3 layer when overlaid duplex oxide or NiO is totally consumed. The kinetics of Cr_2O_3 vaporization are greatly enhanced in the dynamic conditions. The Cr_2O_3 layer can stay intact with the alloy substrate only when protected by NiO or oxide mixture. The depth of inner penetration appears to depend on the extent of Cr depletion in the alloy substrate. It is therefore concluded that in the later stages of oxidation the dynamic oxidation rate is controlled by an interplay between the rate of loss of NiO during the vaporization-reoxidation-condensation process and the rate of formation of the inner Cr_2O_3 scale which halts internal oxidation.

The effect of ThO_2 particles on the observed oxidation behavior is not clear. The dispersive particles may promote the formation of inner Cr_2O_3 layer. The ThO_2 particles which accumulated at the outer edge of oxide mixture (see Figure 4(d)) may temporarily reduce the rate of vaporization of NiO and Cr_2O_3. Additional work, however, is required before any conclusive statement can be made about the effect of ThO_2 on the dynamic oxidation behavior of TD-NiCr. The significance of the formation of porosity (see

Figure 4(b)) in the Cr-depleted substrate is not clear either. The distribution of pore formation is nonuniform, and its effect on the oxidation behavior can not be concluded.

To further enlighten the mechanism proposed for the formation of mushroom type oxide, tests on EP + PO specimens were conducted in Mach-5 flowing N_2 at 2200°F for times ranging from 15 seconds to 1 hour. The objective was to determine the changes in surface oxide morphology resulting from high speed gas flow over the specimen where little or no oxygen was present. X-ray diffraction patterns taken of the exposed specimens showed only NiO and Cr_2O_3 reflections. No nickel or chromium nitride phases were detected. Thermodynamic calculations also indicated the unfavorable formation of nitride phases under the test conditions. Typical micrographs of the exposed specimens are shown in Figure 5. After 15 seconds of exposure, Figure 5(a), there is a rounding of the sharp NiO grain ridges and a development of cavities at the oxide grain boundary regions. These cavities are very similar to those developed during the initial stages of testing in air (see Figure 2) and are presumed to have developed from similar vaporization of NiO. After 10 minutes of exposure there is an increase in the NiO grain size and a further opening up of the cavities in the NiO layer, see Figure 5(b). The NiO layer disappeared first at the original alloy grain boundaries where the NiO layer was thinnest. The exposed boundary regions which are still covered with Cr_2O_3 are clearly visible in Figure 5(c). The Cr_2O_3 oxide phase is stable in the N_2 environment because the formation of volatile CrO_3 is prevented due to the absence of oxygen. The surface NiO disappears totally from the specimen surface at about 1 hour of exposure. The above observations clearly demonstrate that the presence of oxygen is

necessary for the redeposition of NiO on the surface and the subsequent growth of mushroom type oxide.

Mechanical Polished and Preoxidized Surface Finish (MP + PO)

The static oxidation behavior of specimens which were mechanically polished through 600 grit abrasive paper was also studied. After 1 hour of oxidation in air at 1100°C the specimen surface was covered with a layer of globular Cr_2O_3 approximately 1 to 2 μm in thickness (Figure 6). On an etched specimen (not shown in the figure) a thin layer (0.3 μm or less) of fine-grain recrystallized alloy was observed adjacent to the external oxide. The existance of this recrystallized layer was also confirmed by X-ray diffraction analysis. The {111} reflection which was not detectable from the specimen before preoxidation was measurable after oxidation (see Table I).

When MP + PO specimens were exposed to the dynamic environment, the external Cr_2O_3 was further oxidized to form volatile CrO_3. Scanning micrographs and X-ray diffraction patterns taken of short time exposure specimens indicated that the Cr_2O_3 layer was nearly totally vaporized after approximately 15 seconds. The rate of evaporization was greatly enhanced by the flowing conditions, particularly with the presence of atomic oxygen in the air stream. As Cr_2O_3 disappeared from the surface, a thin layer of NiO started to form at the Ni-rich alloy surface. The formation of a NiO layer essentially sealed off rapid Cr loss through vaporization. During subsequent oxidation rapid external growth of this NiO layer was observed.

Photographs shown in Figure 7 were taken of MP + PO specimens after 1 and 10 minutes of oxidation. After 1 minute of exposure, the specimen

surface was covered with a porous mushroom type NiO oxide (Figure 7(a) and (b)). The cross-sectional micrograph shows that the mushroom oxide grows on top of a relatively solid NiO layer which is formed by external growth. Under the NiO layer a duplex oxide layer resulting from internal oxidation is observed. The fine-grain recrystallized surface layer provides for numerous quick paths for internal oxidation, and hence delays the formation of a continuous inner Cr_2O_3 layer. At this stage of oxidation, no inner Cr_2O_3 layer has yet formed at the oxide/alloy interface. As oxidation proceeds, however, a continuous Cr_2O_3 layer is eventually developed, and internal oxidation effectively stops. Mushroom oxide clusters continue to grow at the expense of the underlaid NiO. Experimental evidence of this is provided by the micrographs shown in Figure 7(c) and (d), which were taken from a 10 minute exposure specimen. Oxidation then proceeds in the same sequence as that previously presented for the EP + PO specimens. It should also be noted that the oxidation behavior here described is similar to that reported in the preceeding paper[19] for specimens with belt-sanded surface finishing. There is, however, a difference in the depth of internal oxidation at the early stages of oxidation (1-3 minutes). The belt-sanded finishing resulted in deeper penetration presumably because of a thicker recrystallized surface layer in the alloy substrate.

The MP + PO specimens were also tested in a flowing N_2 environment. At 15 seconds of exposure no changes in Cr_2O_3 morphology were detected. At 10 minutes of exposure, however, changes in the Cr_2O_3 topology were observed. A typical micrograph is given in Figure 8(a). X-ray diffraction analysis indicated that the surface layer shown in the picture is Cr_2O_3, apparently the remains of the original Cr_2O_3 oxide formed during static preoxidation. Grimley et al.[22] reported that the vaporization of Cr_2O_3

under neutral conditions proceeds with the formation of Cr, CrO, CrO_2, O, and O_2 as the principal gaseous species. Under oxidizing conditions CrO_3 was observed. During the flowing N_2 tests, oxidation of Cr_2O_3 to form volatile CrO_3 should not have occurred. The Cr_2O_3 oxide appears in the shape of mushroom type morphology with small solid pillars sticking up from the alloy substrate. Careful comparison of photographs taken before and after exposure suggests that the small pillars observed in Figure 8(a) are the remains of the original Cr_2O_3 globules which grew relatively large during preoxidation. It is apparent that the high speed flowing conditions results in accelerated vaporization of Cr_2O_3 at the regions which are generally below the general level of the surface.

The MP + PO specimen after 10-minute N_2 exposure was again oxidized in flowing air conditions. Immediately upon exposure a sudden glow at the shock wave was detected, presumably the result of rapid vaporization of the Cr_2O_3 pillars. A typical micrograph taken from the 10-minute N_2 exposure specimen after an additional 5 minutes of air exposure is shown in Figure 8(b). The surface is uniformly covered with NiO clusters typical of the type of morphology found for short time air tests. This is precisely what was expected to happen, and can be readily explained by the oxidation events previously discussed.

Electropolished Surface Finishing (EP)

When EP specimens were exposed to the dynamic environment, both NiO and Cr_2O_3 formed initially at the specimen surface. However, because of a high vaporization rate of Cr_2O_3 and rapid growth rate of NiO, the formation of NiO prevailed during subsequent oxidation. The NiO was immediately converted into mushroom type morphology. The external growth of NiO leads

to the development of a thin Cr-rich alloy substrate which promoted the formation of a uniform Cr_2O_3 layer under the outer porous NiO. This is illustrated in Figure 9(a) and (b), which show the micrographs taken of a 1 minute exposure specimen. The entire surface, except the alloy grain boundary regions, is covered with mushroom type oxide clusters. Although the NiO mushrooms are porous, they do serve to protect the underlying Cr_2O_3 from rapid vaporization. At this stage of oxidation, the Cr-depleted zone in the substrate is small and no recrystallization is expected to occur at the specimen surface. Consequently, the NiO and Cr_2O_3 duplex oxide layer is not detected. As the oxidation process proceeds, both the number and size of NiO mushroom clusters decrease, and the Cr_2O_3 layer becomes thinner. The surface and cross-section of a 10-minute exposure specimen is shown in Figure 9(c) and (d). Apparently, the porous NiO is still protecting the underlying Cr_2O_3. A steep Cr-depleted zone, which extended 5-10 μm into the alloy substrate, was detected. At some localized regions, especially at the edges of specimens, islands of large NiO mushrooms were observed. Local oxidation penetration was always found under the NiO islands. After 2 hours of oxidation the specimen surface was covered with a layer of large clusters. The oxide morphology and oxide cross-section were very similar to those observed on EP + PO or MP + PO specimens which had been oxidized for 10 minutes. It is apparent that the oxidation rate of EP specimens is slower than that of specimens with EP + PO or with MP + PO pretreatments.

Mechanical Polished Surface Finish (MP)

The micrographs shown in Figure 10(a) and (b) were taken of MP specimens after 1 minute of oxidation. Scattered islands of mushroom NiO are observed

on the surface. Away from the islands small NiO clusters are observed to grow on ridges of scratches left on the surface from the mechanical polishing. In Figure 10(b), internal oxidation typical of that observed on MP + PO specimen at 1 minute of exposure is detected under the mushroom islands. Small NiO clusters growing atop of a Cr_2O_3 layer typical of EP specimens after 1 minute of oxidation are observed at regions away from the mushroom islands. It is believed that this non-homogeneous oxidation results from concurrent oxidation and recrystallization at the surface. The detection of a medium intensity {111} reflection from the specimen after 15 seconds of exposure, see Table I, indicates that recrystallization takes place at the very early stage of oxidation. Since recrystallization is a thermally-activated process, it should occur non-uniformly at the deformed surface layer. The fine grained recrystallized layer provides for numerous nucleation sites for selective oxidation of Cr_2O_3. At areas where recrystallization takes place rapidly, an external Cr_2O_3 layer forms at the surface upon exposure. Consequently, the early stage oxidation is similar to that of MP + PO specimens. At regions where recrystallization proceeds at a slow rate, an external NiO and an inner Cr_2O_3 layer form at the surface immediately upon exposure. The oxidation is therefore following a process similar to that described for the EP specimens. After 10 minutes of oxidation, large NiO mushrooms are fully developed, see Figure 10(c) and (d). At some localized regions, however, small mushrooms growing atop the Cr_2O_3 layer are still visible.

Discussion

High temperature technology has now advanced to the point where significant atomic gas concentration is frequently encountered, particularly in subatmospheric pressure conditions. During a crucial part of space shuttle re-entry the thermal protection shield materials will experience a temperature maximum (1000^{o}-1200^{o}C for TD-NiCr), and a large fraction of the boundary layer oxygen will be dissociated by the shockwave. The fraction of dissociated oxygen ranges from 0 to 100%, depending on altitude and angles of entry attack[13,14]. In high-energy propulsion, the combustion exhaust product can also contain appreciable amounts of highly reactive species[23]. Under the arc-jet conditions employed in the present study the concentration of atomic oxygen at the specimen surface was reported to be approximately 0.5%, according to simple stream enthalpy calculation[24]. Electrical arcing in the arc chamber may produce additional oxygen atoms. Although arc-jets produce an environment high in ionized gases and low in atomic oxygen relative to those encountered in re-entry, they do provide a better re-entry simulation than any other facility available. The dissociated oxygen, although low in concentration, may impose significant variation in oxidation kinetics of metals. Results of Dickens et al.[25] indicated that the introduction of 0.02% atomic oxygen in the oxidizing environment at 710^{o}C increases the oxidation rate of pure Ni by a factor of 14 over that observed in molecular oxygen. Results of Gilbreath[13,14] also demonstrated the accelerated oxidation of space shuttle TPS metals in flowing air (12 m/sec) which contained a significant amount of atomic oxygen. Metal degradation measured in terms of metal recession was about two orders of magnitude greater in atomic oxygen than in static oxygen, and about one order greater than caused by flowing molecular oxygen. In static and

flowing O_2, dark-grey and adhesive surface scale rich in Cr was detected. In flowing O, yellow-green, brown and friable scale rich in Ni was observed. The external mushroom type NiO oxide formed during the present dynamic testing is invariably yellowish to greenish white. The mushroom oxide was very friable and a sharp tap or slight bending of the specimen caused much of the oxide to spall. Based on the similarity of visual appearance and oxide identity observed in atomic oxygen and in arc-jet, it is suggested that the dissociated oxygen in the arc-jet air stream plays the most important role in the development of mushroom type oxide morphology.

It has been well established that the vaporization of Cr_2O_3 under high temperature dry oxidation conditions occurs with the formation of CrO_3 vapor species[22,26-30]. In static conditions, the oxidation rate of TD-NiCr, as well as other metals forming Cr_2O_3 as an external protective scale, is initially controlled by an interplay between Cr diffusion through Cr_2O_3 and the formation of gaseous CrO_3. However, after the Cr_2O_3 scale reaches its steady-state thickness, the oxidation rate becomes linear and equal to that of vaporization process[8,27]. The rate of vaporization in turns depends on mass transport of reaction products through the stagnant boundary layer, temperature, oxygen partial pressure, and total pressure[27-31]. Under flowing environments, the reaction product is continuously swept away by flowing gas. In hypervelocity flow, the vaporization rate may therefore approach the theoretical maximum given by Hertz-Langmuir equation[29,30]:

$$G_i = \frac{\alpha_i P_i}{2.256 \times 10^{-2}} \left(\frac{M_i}{T}\right)^{\frac{1}{2}}$$

where G_i is the weight loss of ith species in gm/cm^2-sec., P_i is vapor pressure in atmospheres, M_i is molecular weight in grams, T is temperature

in ^{o}K, and α_i is vaporization coefficient defined as the ratio of observed vaporization rate under the given conditions to that of the maximum possible rate. Taking P_{CrO_3} to be 3×10^{-7} from data of Kohl et al( ), and assuming α_{CrO_3} to be unity which is reasonable for the present Mach-5 air flow condition where no redeposition of Cr_2O_3 is likely to occur, the vaporization rate of CrO_3 was calculated to be 3.8×10^{-6} gm/cm^2-sec, corresponding to a thickness reduction of Cr_2O_3 at 7.3×10^{-3} μm/sec. This is about 2 orders of magnitude less than that observed in the present study where the external Cr_2O_3, 2 μm in thickness, on MP + PO specimen, is totally evaporized at 15 seconds of exposure (it should also be recalled that it takes about 10-12 seconds to heat the specimen to test temperature). These observations suggest that under the arc-jet conditions the surface reaction rate determines the vaporization kinetics of the Cr_2O_3 layer. The dissociated oxygen in the air stream greatly enhances the oxidation of Cr_2O_3 to form CrO_3, thereby producing an increased vaporization rate.

A calculation of maximum vaporization rate of NiO was also attempted. Since the major vapor species over NiO(s) under neutral conditions are Ni(v) and O, the partial pressure of Ni(v) or O, which is 2×10^{-8} atm at 1200°C[21], was used. Assuming no redeposition occurs, the maximum rate was found to be 2×10^{-7} gm/cm^{2}sec, corresponding to 3×10^{-3} μm/sec thickness recession of NiO. This roughly agrees with the present observation that a layer of external NiO approximately 3 μm in thickness was essentially totally evaporized after about 1 hour of exposure to the flowing N_2 environment. Reduced vaporization is expected in oxidizing environments as a result of increasing NiO redeposition. With the much greater vaporization rate of Cr_2O_3 over that of NiO in the arc-jet, it is anticipated that NiO would be the external oxide. The rate of NiO loss through the vaporization-deposition process is therefore one of the rate

controlling factors. This is also supported by the results of Gilbreath[13] which indicates that greater weight loss occurs in dilute atomic oxygen than at higher atomic oxygen concentrations (~40%). Apparently, a maximum oxidation rate occurs at a low concentration of dissociated oxygen, below which enhanced vaporization of Cr_2O_3 predominates and above which redeposition of NiO predominates.

Surface pretreatment has a significant effect on the early stage oxidation behavior of TD-NiCr alloy. Mechanical polishing leads to surface recrystallizati at the very early stages of oxidation. Under the dynamic environment, the recrystallized layer provides numerous quick paths for internal oxidation which delays the formation of an inner Cr_2O_3 layer, thereby increasing the initial rate of metal recession. Removal of the surface deformation layer by electropolishing slows down the initial rate of oxidation for the same test conditions. However, electropolishing produces a surface condition with reduced emissivity, a condition which would result in an increased heat shield temperature under the same re-entry conditions. Static pre-oxidation of MP specimen generates an external Cr_2O_3 layer which has a relatively high emissivity; but the Cr_2O_3 layer is quickly evaporized when exposed to the flowing air. Preoxidation of EP specimen produces a faceted NiO which is quickly converted into mushroom type morphology. The influence of surface pretreatment becomes insignificant after about 2 hours of oxidation. At this later stage, local oxidation following a cyclic process is the predominant mechanism. The oxidation model proposed in the previous study[19] can be used to explain the details involved during the oxidation process.

These results agree with those reported by Lowell et al[15] who found that NiO was the equilibrium external oxide formed on TD-NiCr tested in a

Mach-1 burner rig at 1200°C. They also reported that surface pretreatment becomes insignificant after about 1 hour of oxidation. They have proposed an oxidation model and concluded that diffusion of Cr through NiO is the limiting step. Goldstein[31] has developed an analytical model that described the ablation of TD-NiCr in hypersonic flow. The model accounted for diffusion controlled and sublimation rate controlled reaction of Cr_2O_3 to gaseous products. Vaporization of NiO was not considered in the development of the model. Based on the results of this investigation and those reported by Lowell et al.[15] it appears that a more detailed analysis which takes into account NiO vaporization and internal oxidation is required to more accurately describe the oxidation kinetics.

Conclusions

Based on the observations described herein, together with the results reported in the previous study[19] and in the literature, the following conclusions can be made.

(1) The atomic oxygen which is generated through dissociation of molecular oxygen by the shock wave plays the most important role in oxidation of TD-NiCr alloy under the arc-jet environment.

(2) The rate of Cr_2O_3 vaporization by formation of gaseous CrO_3 is greatly accelerated by the dynamic conditions. Cr_2O_3 oxide provides good oxidation protection only when protected by NiO.

(3) NiO is the stable external oxide found under the flowing air conditions. The typical microstructure consists of an external layer of NiO with a porous mushroom type morphology, an intermediate layer of NiO and Cr_2O_3 oxide mixture, and a continuous inner Cr_2O_3 layer in contact with Cr-depleted alloy substructure. The development of NiO mushroom type oxide follows three steps: (a) vaporization of NiO predominantly by dissociation into Ni vapor and O atoms, (b) reoxidation of Ni vapor primarily with dissociated oxygen in air stream, and (c) condensation of NiO at elevated sites on specimen surface. The mushroom oxide clusters grow at the expense of underlying NiO, and fade when the supply of Ni is limited.

(4) Surface pretreatment has a significant influence on the topography, order and relative amount of NiO and Cr_2O_3 formed during the early stages of oxidation, but becomes less important as exposure time increases. Mechanical polishing induces surface recrystallization, and therefore enhances initial substrate recession at the very early stages of oxidation. Removal of the surface deformation layer by electropolishing slows down the initial oxidation rate.

(5) Despite various surface preparations, the oxidation behavior of the alloy at later stages of oxidation can be characterized by local oxidation following a cyclic process which consists of (a) rapid internal oxidation of unprotected Cr-depleted alloy substrate until an inner Cr_2O_3 layer forms, (b) growth and vaporization of NiO mushroom oxide with concurrent vaporization of any Cr_2O_3 in the outer oxide mixture, and (c) rapid vaporization of inner Cr_2O_3 when overlaid oxide mixture is totally consumed. The rate of oxidation is controlled by the rate of loss of NiO during the vaporization-condensation process, and by the rate of formation of inner Cr_2O_3 layer. The critical value of Cr concentration for the formation of continuous inner Cr_2O_3 appears to be approximately 15% for TD-NiCr oxidized at 1200°C.

Acknowledgments

The authors are grateful to the National Aeronautics and Space Administration, Langley Research Center, Hampton, Virginia, for their support of this research.

References

1. B. A. Wilcox and A. H. Clauer, Metal Science Journal, 1969, Vol. 3, pp. 26-33.

2. B. A. Wilcox, A. H. Clauer and W. S. McCain, Trans. AIME, 1969, Vol. 293, pp. 1791-1795.

3. B. A. Wilcox and A. H. Clauer, NASA CR-2025, 1972.

4. K. H. Holko, NASA TM-X-52952, 1971.

5. W. A. Sanders and C. A. Barret, NASA TM X-67864, 1971.

6. G. R. Wallwork and A. Z. Hed, Oxidation of Metals, 1971, Vol. 3, No. 3, p. 229-241.

7. J. Stringer, B. A. Wilcox and R. I. Jaffee, Oxidation of Metals, 1972, Vol. 5, No. 1, pp. 11-47.

8. C. S. Giggins and F. S. Pettit, Met. Trans., 1971, Vol. 2, pp. 1071-1078.

9. H. H. Davis, H. C. Graham and I. A. Kvernes, Oxidation of Metals, 1971, Vol. 3, No. 5, pp. 431-451.

10. C. E. Lowell, D. L. Deadmore, S. J. Grisaffe, and I. L. Drell, NASA TN D-6290, 1971.

11. C. S. Giggins and F. S. Pettit, Trans. AIME, 1969, Vol. 245, pp. 2495-2507.

12. C. S. Giggins and F. S. Pettit, Trans. AIME, 1969, Vol. 245, pp. 2509-2514.

13. W. P. Gilbreath, NASA TM X-62064, 1971.

14. W. P. Gilbreath, Progress in Astronautics and Aeronautics, 31, 1972, pp. 127-143.

15. C. E. Lowell and W. A. Sanders, NASA TN D-6562, 1971.

16. J. R. Johnston and R. L. Ashbrook, NASA TN D-5376, 1969.

17. F. J. Centolanzi, NASA TM X-62015, 1971.

18. F. J. Centolanzi, H. B. Probst, C. E. Lowell and N. B. Zimmerman, NASA TM X-62092, 1971.

19. D. R. Tenney, C. T. Young and H. W. Herring, Met. Trans., 1974, vol. 5, pp. 1001-11.

20. J. W. Colby, MAGIC IV Program, Bell Telephone Lab., Inc., 1971.

21. R. T. Grimley, R. P. Burns and M. G. Inghram, J. of Chem. Phys., 1961, Vol. 35, No. 2, pp. 551-554.

22. R. T. Grimley, R. P. Burns and M G. Inghram, J. of Chem. Phys., 1961, Vol. 34, No. 2, pp. 664-667.

23. D. E. Rosner and H. D. Allendorf, High Temp. Technology, Butterworths, London, 1967, pp. 707-719.

24. "Instructions and Operating Procedures for Aerotherm 100 KW Constrictor Arc Heater System," Aerotherm Corporation, Tech. Narrative Report No. IM-68-1, NASA Contract No. NAS1-7560, 1968.

25. P. G. Dickens, R. Heckingbottom and J. W. Linnett, Trans. Faraday Soc., 1969, Vol. 65, pp. 2235-2247.

26. D. Caplan and M. Cohen, J. Elec. Soc., 1961, Vol. 108, pp. 438-442.

27. C. S. Tedmon, Jr., J. Elec. Soc., 1966, Vol. 113, pp. 766-769.

28. H. C. Graham and H. H. Davis, J. Amer. Cer. Soc., 1971, Vol. 54, pp. 89-93.

29. F. J. Kohl and C. A. Stearns, NASA TM X-52879, 1970.

30. R. A. Rapp, AGARD-CP-120, 1973, pp. 147-154.

31. H. E. Goldstein, AIAA Paper No. 71-34, 1971

List of Figure Captions

Figure 1. (a) Oxide morphology and (b) oxide cross section of electropolished and preoxidized (one hour in static air at 2000°F) specimen. Energy dispersive X-ray analyses were made of the different oxide layers shown in (b) indicating variation of Cr, Ni and Th contents.

Figure 2. Topography of external NiO formed on electropolished and preoxidized specimens after (a) 12 seconds, and (b) 15 seconds of exposure to a 2200°F, Mach-5 and 0.002 lb/sec. flowing air environment. (c) Higher magnification micrograph of central area in (b).

Figure 3. Surface morphology and oxide cross sections of electropolished and preoxidized specimens after (a), (b) 1 minute, and (c), (d) 10 minutes of dynamic oxidation.

Figure 4. Typical oxide topography and oxide cross sections observed on electropolished and preoxidized specimen after two hours of exposure to the dynamic environment. Probe scan was made along the line marked with an arrow in (c).

Figure 5. Surface topography of electropolished and preoxidized specimen after (a) 15 seconds, and (b) 10 minutes of exposure to a Mach-5, 2200°F and 0.002 lb/sec. flowing N_2 gas. (c) a lower magnification micrograph of 10 minutes exposure specimen.

Figure 6. Morphology of external Cr_2O_3 and oxide cross section of mechanically polished and preoxidized (one hour in static air at 2000°F) specimen.

Figure 7. Oxide topography and cross sections of mechanically polished and preoxidized specimens after (a), (b) 1 minute, and (c), (d) 10 minutes of dynamic oxidation.

Figure 8. Surface morphology of mechanically polished and preoxidized specimen after (a) 10 minutes of exposure to flowing N_2 gas, and (b) subsequent 5 minutes exposure to flowing air environment.

Figure 9. Oxide topography and cross sections of electropolished specimens after (a), (b) 1 minute, and (c) (d) 10 minutes of dynamic oxidation.

Figure 10. Oxide morphology and cross sections of mechanically polished specimens after (a), (b) 1 minute, and (c), (d) 10 minutes of dynamic oxidation.

TABLE I

OXIDES DETERMINED BY X-RAY DIFFRACTION ON TD-NiCr EXPOSED AT 2200°F IN HIGH GAS VELOCITY OXIDATION APPARATUS FOR VARIOUS TIMES

	Alloy Substrate		Adhering Surface Oxides									
			ThO_2				Cr_2O_3			NiO		
	(111)	(200)	(111)	(200)	(220)	(311)	(012)	(104)	(110)	(111)	(200)	(220)
EP 1 min		VS	W	VW	VW	VW	VW	M	VW	W	S	W
EP 10 min		VS	W	VW	VW	VW	VW	W		W	M	W
EP 2 hrs		S	M	W	W	W	VW	VW		S	S	S
EP+PO		VS								S	VS	S
EP+PO 30 Sec		VS								S	VS	S
EP+PO 1 min		VS								S	VS	S
EP+PO 3 min		VS								S	VS	S
EP+PO 10 min		VS	M	W	W		W	W	W	W	M	W
EP+PO 30 min		VS	W			VW	VW	W	W	M	VS	M
EP+PO 2 hrs		VS	M	M		VW	VW	W	W	M	S	W
EP+PO 10 hrs		VS	S	M		M	VW	W	W	M	M	W
MP 15 sec	M	VS	W	VW	VW	VW	VW					
MP 1 min	M	VS	W	VW	VW	VW				VW	VW	
MP 10 min	M	VS	W	VW	VW	VW	VW	W	W	M	S	M
MP 2 hrs	VW	S	M	W	W	W	VW	W	VW	M	M	W
MP+PO	S	VS	M	W	W	W	W	M				
MP+PO 1 min	W	VS	W				VW	W		S	S	S
MP+PO 2 hrs		VS	M	W	W	W	W	W	VW	M	M	W
MP+PO 10 hrs		VS	S	M	M	M	W	W	VW	M	M	M

EP = Electropolished; EP+PO = Electropolished and Preoxidized; MP = Mechanical Polished MP+PO = Mechanical Polished and Preoxidized

VS = Very Strong; S = Strong; M = Medium; W = Weak; VW = Very Weak; Blank = Not Detected

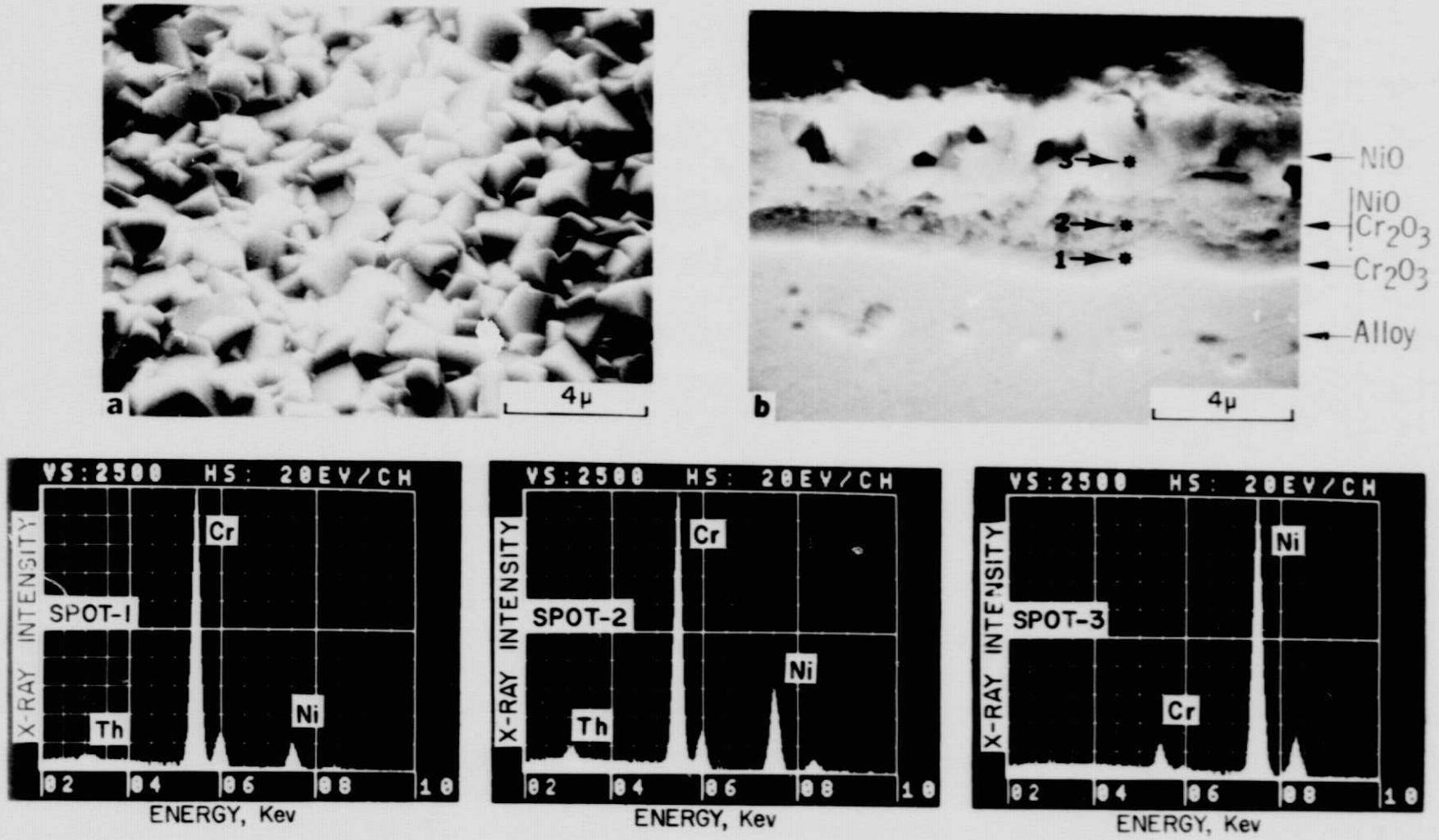

Figure 1. (a) Oxide morphology and (b) oxide cross section of electropolished and preoxidized (one hour in static air at 2000°F) specimen. Energy dispersive X-ray analyses were made of the different oxide layers shown in (b) indicating variation in Cr, Ni and Th contents.

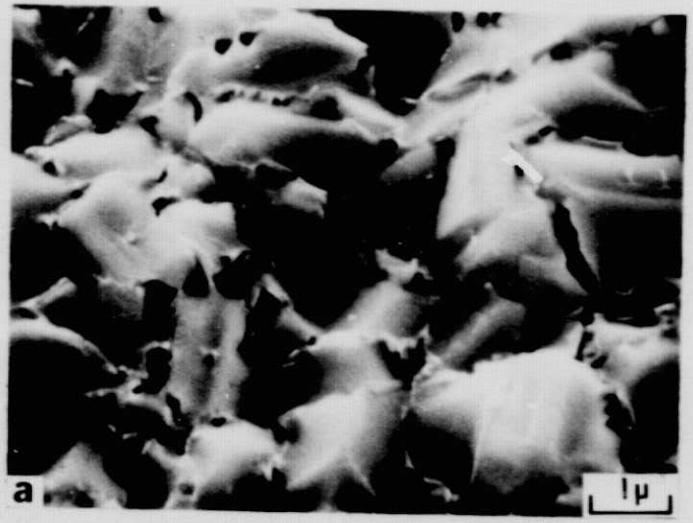

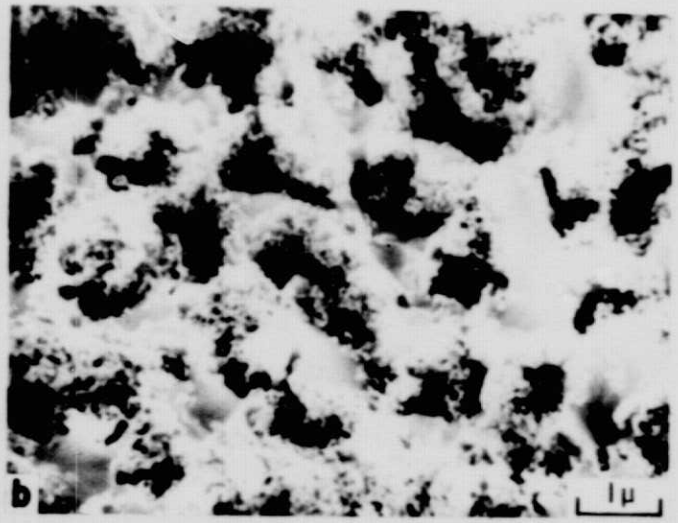

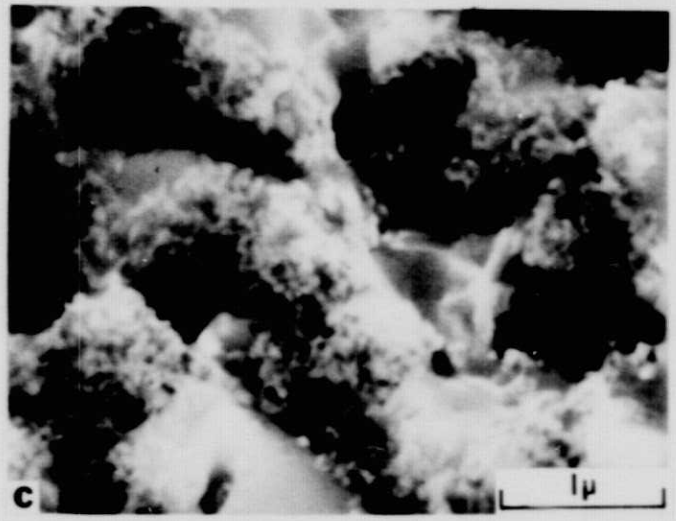

Figure 2. Topography of external NiO formed on electropolished and preoxidized specimens after (a) 12 seconds, and (b) 15 seconds of exposure to a 2200°F, Mach-5 and 0.002 lb/sec. flowing air environment. (c) Higher magnification micrograph of central area in (b).

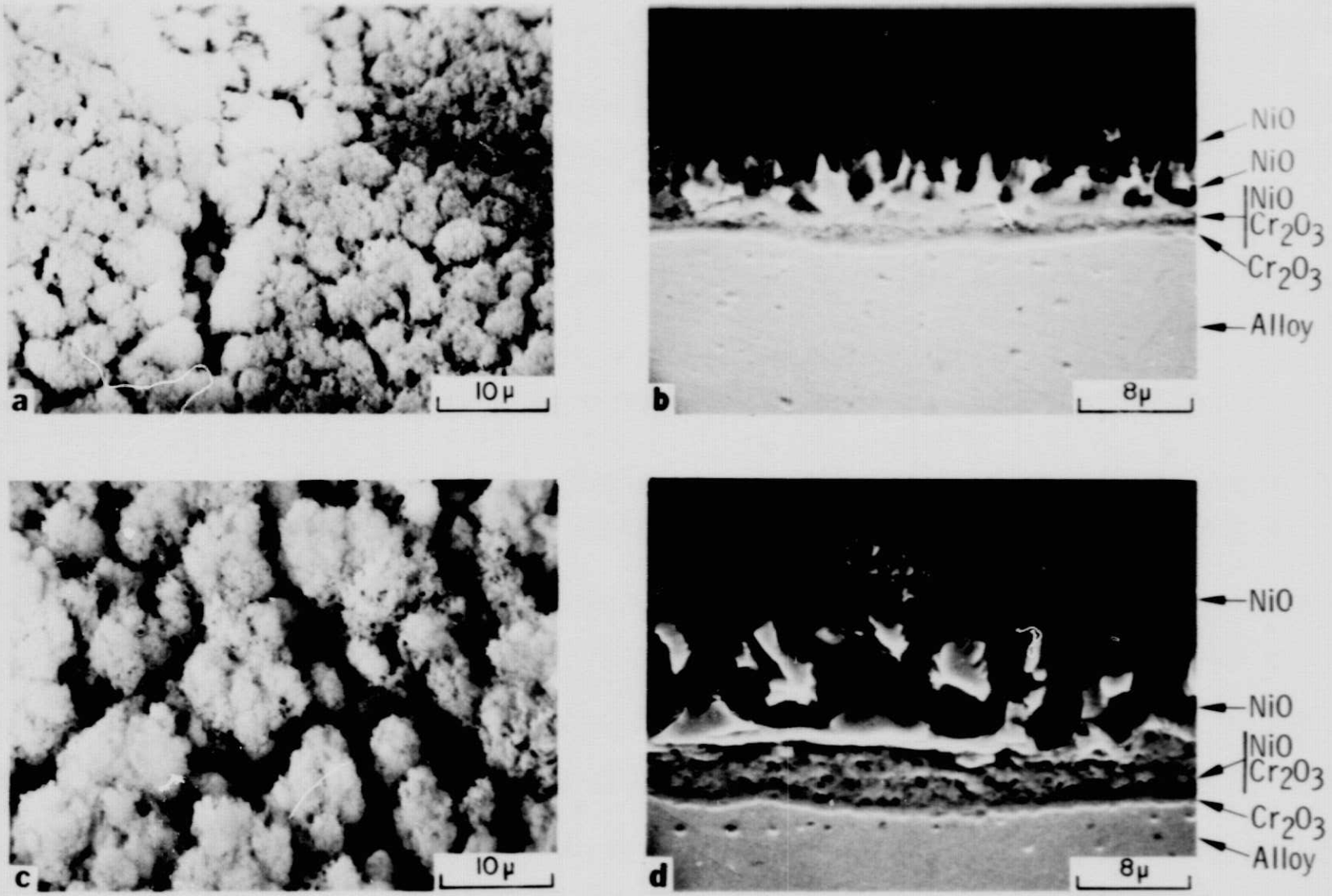

Figure 3. Surface morphology and oxide cross sections of electropolished and preoxidized specimens after (a), (b) 1 minute, and (c), (d) 10 minutes of dynamic oxidation.

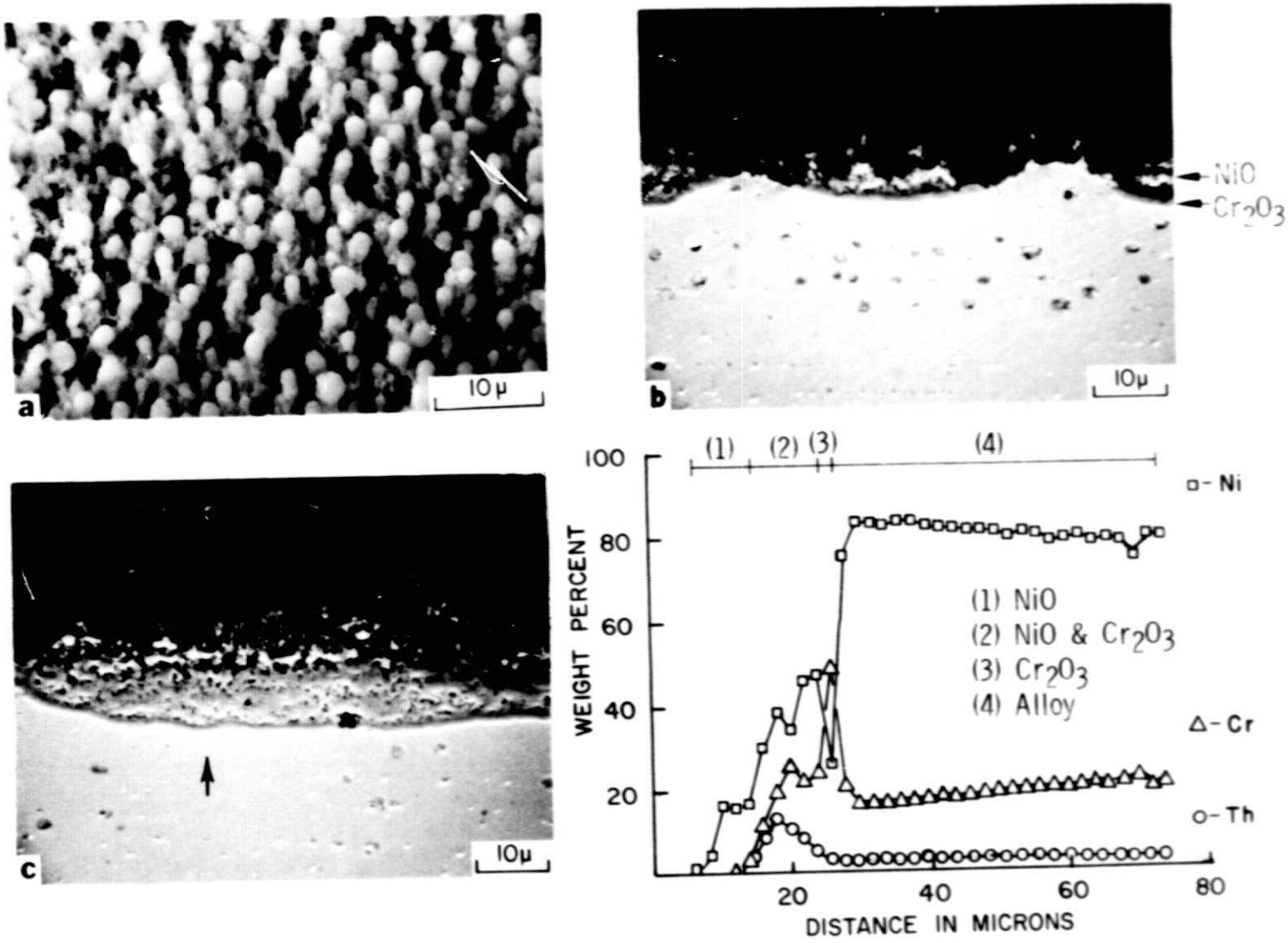

Figure 4. Typical oxide topography and oxide cross sections observed on electropolished and preoxidized specimen after two hours of exposure to the dynamic environment. Probe scan was made along the line marked with an arrow in (c).

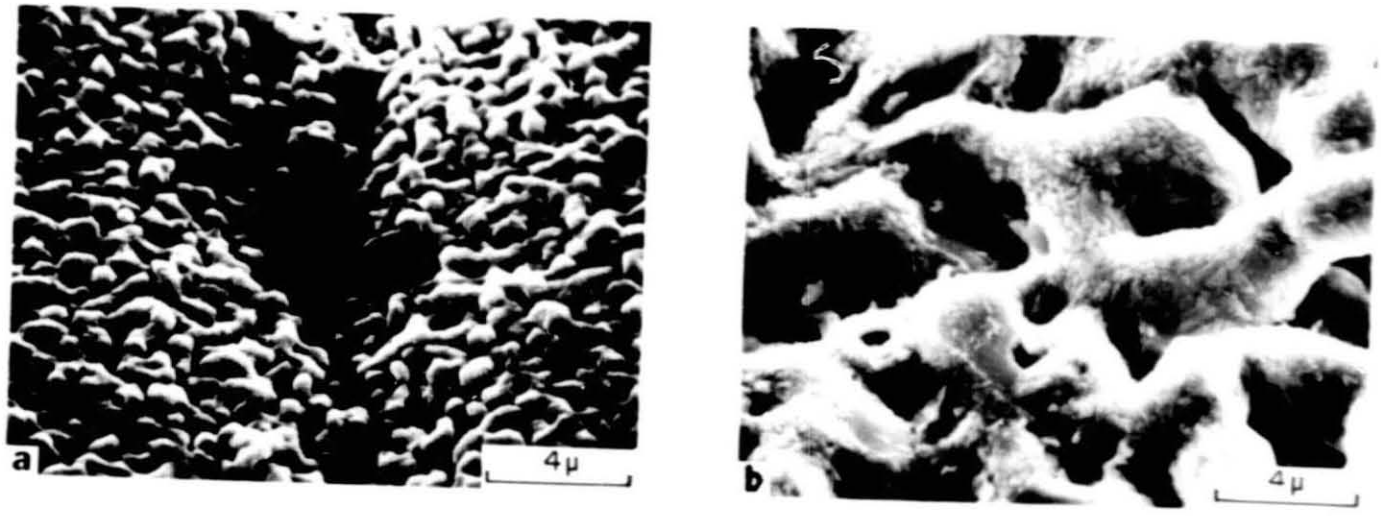

Figure 5. Surface topography of electropolished and preoxidized specimen after (a) 15 seconds, and (b) 10 minutes of exposure to a Mach-5, 2200^{0}F and 0.002 lb/sec. flowing N_2 gas. (c) A lower magnification micrograph of 10 minutes exposure specimen.

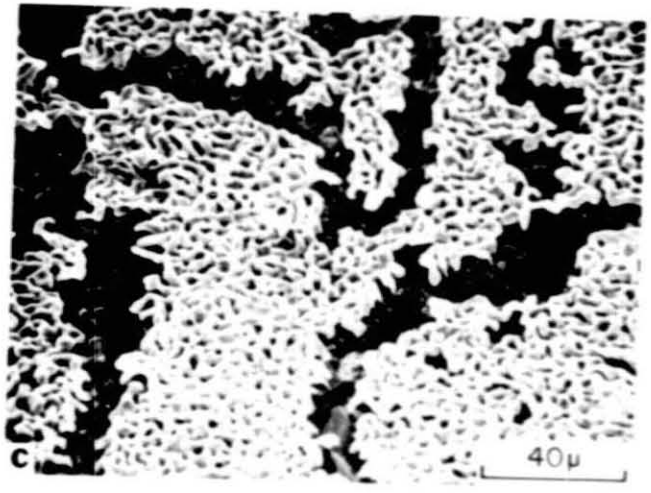

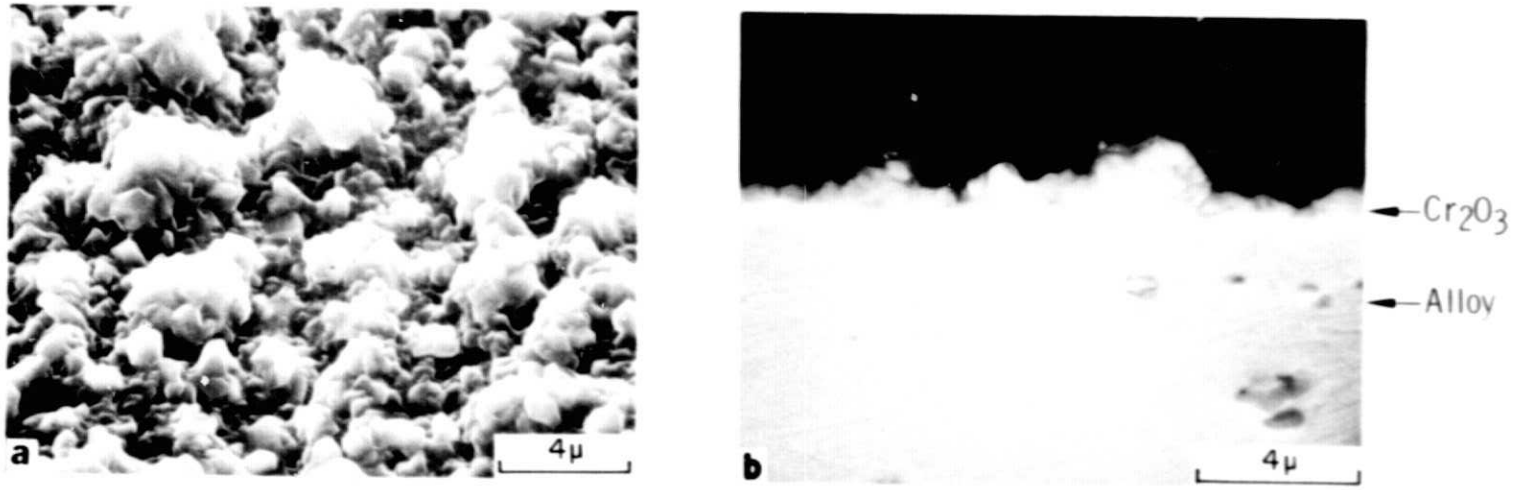

Figure 6. Morphology of external Cr_2O_3 and oxide cross section of mechanically polished and preoxidized (one hour in static air at 2000°F) specimen.

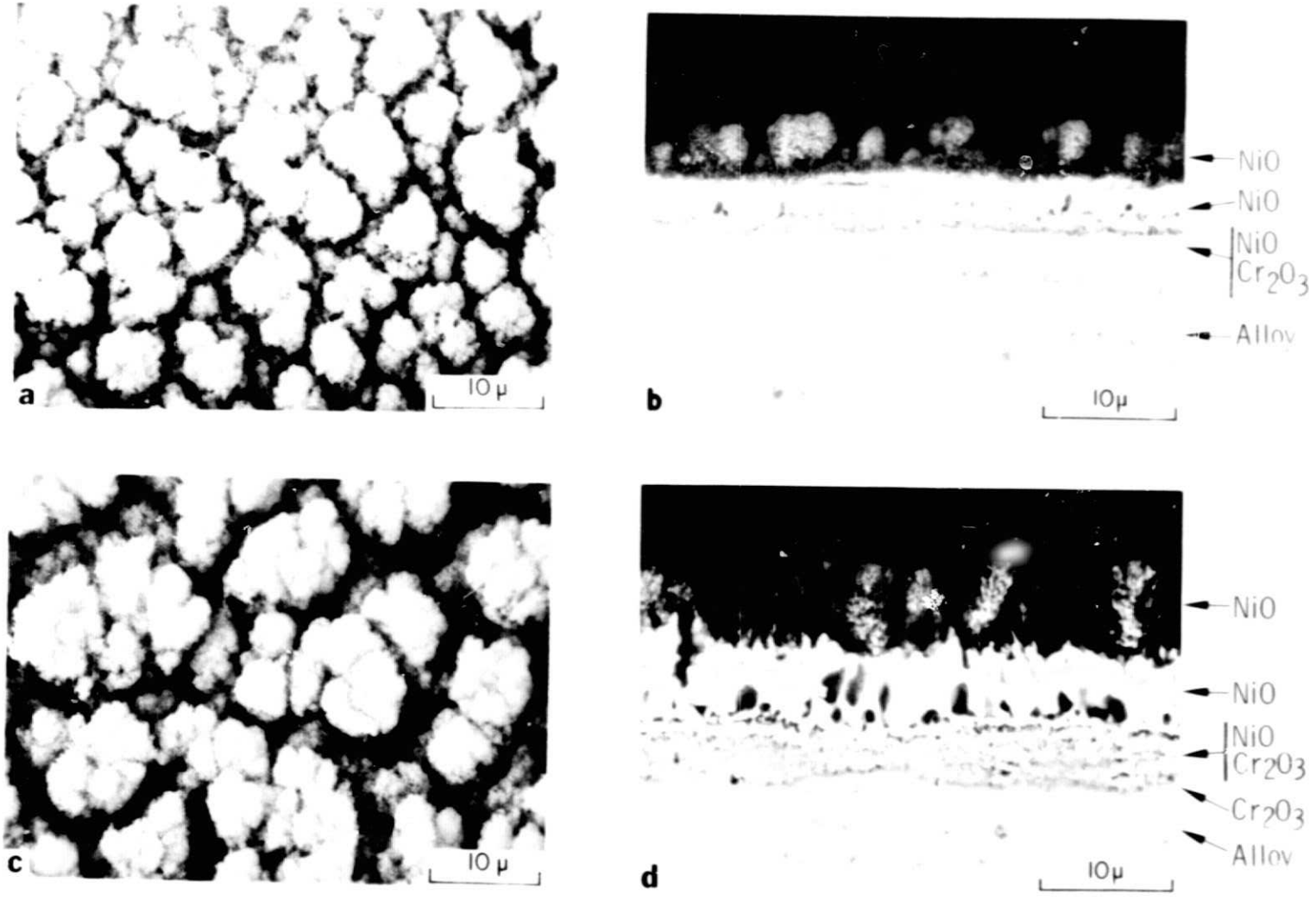

Figure 7. Oxide topography and cross sections of mechanically polished and preoxidized specimens after (a), (b) 1 minute, and (c), (d) 10 minutes of dynamic oxidation.

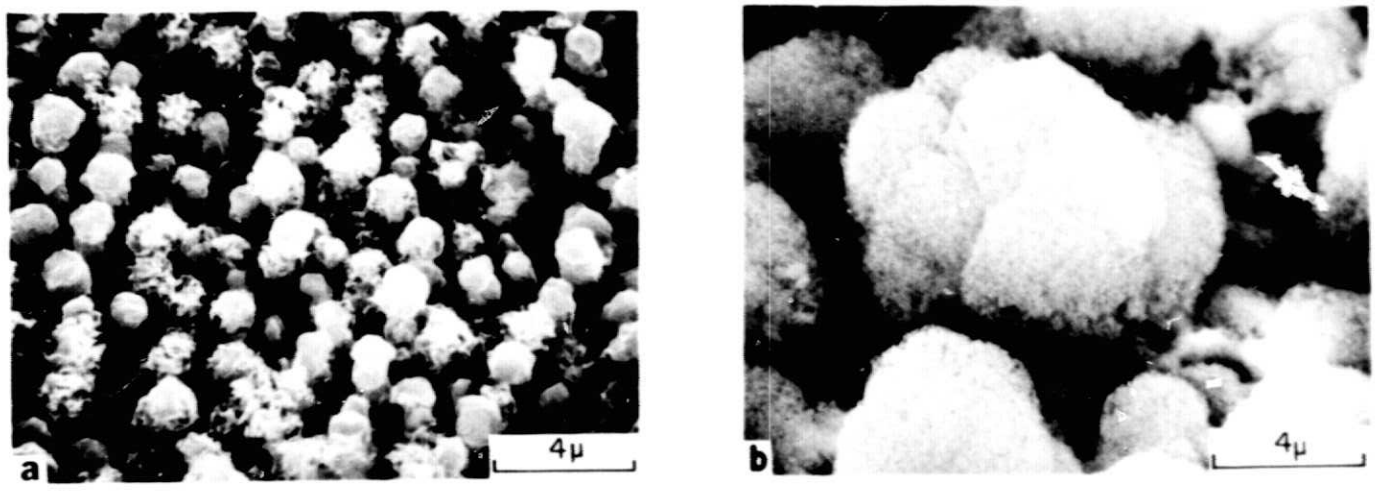

Figure 8. Surface morphology of mechanically polished and preoxidized specimen after (a) 10 minutes of exposure to flowing N_2 gas, and (b) subsequent 5 minutes exposure to flowing air environment.

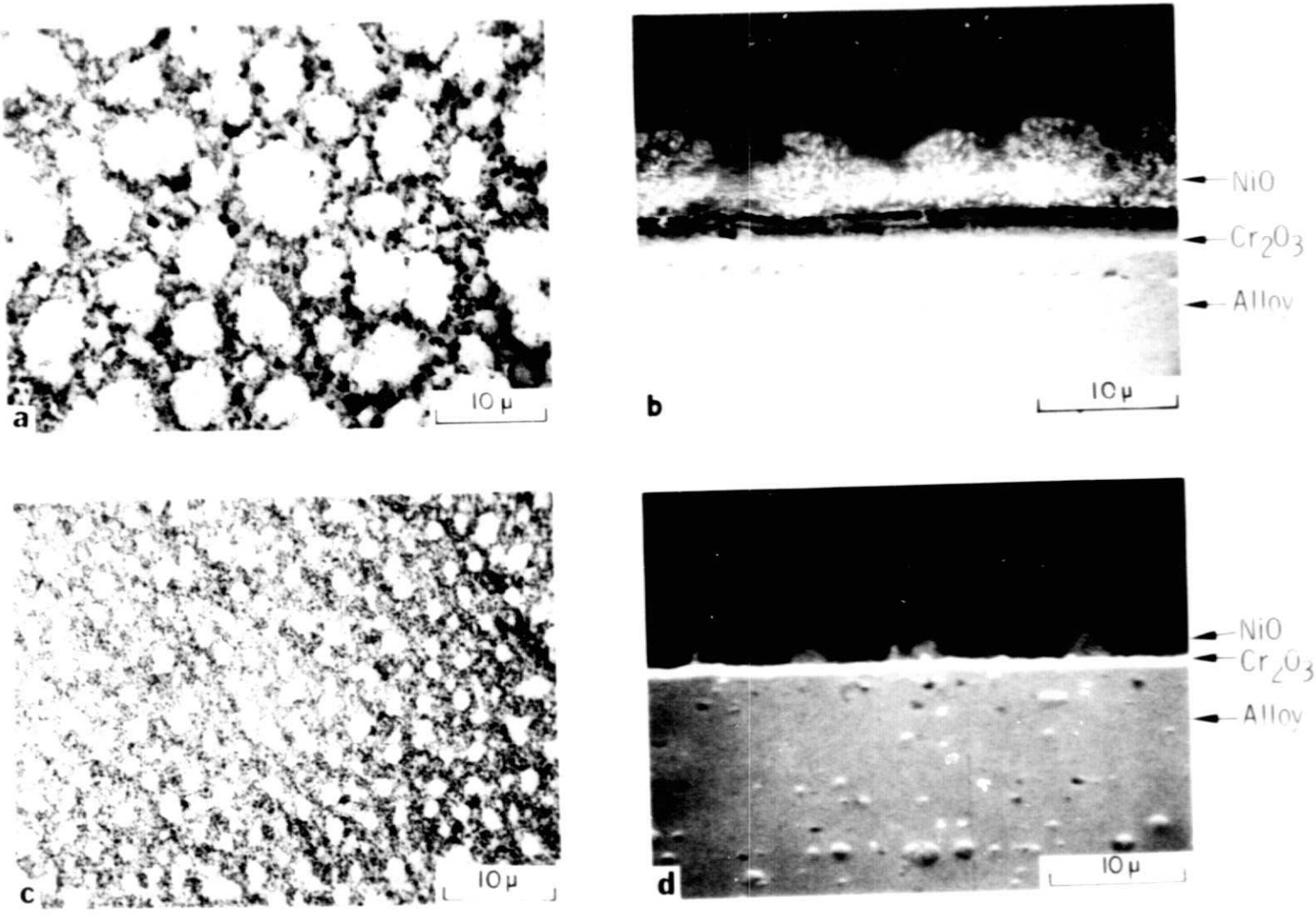

Figure 9. Oxide topography and cross sections of electropolished specimens after (a), (b) 1 minute, and (c), (d) 10 minutes of dynamic oxidation.

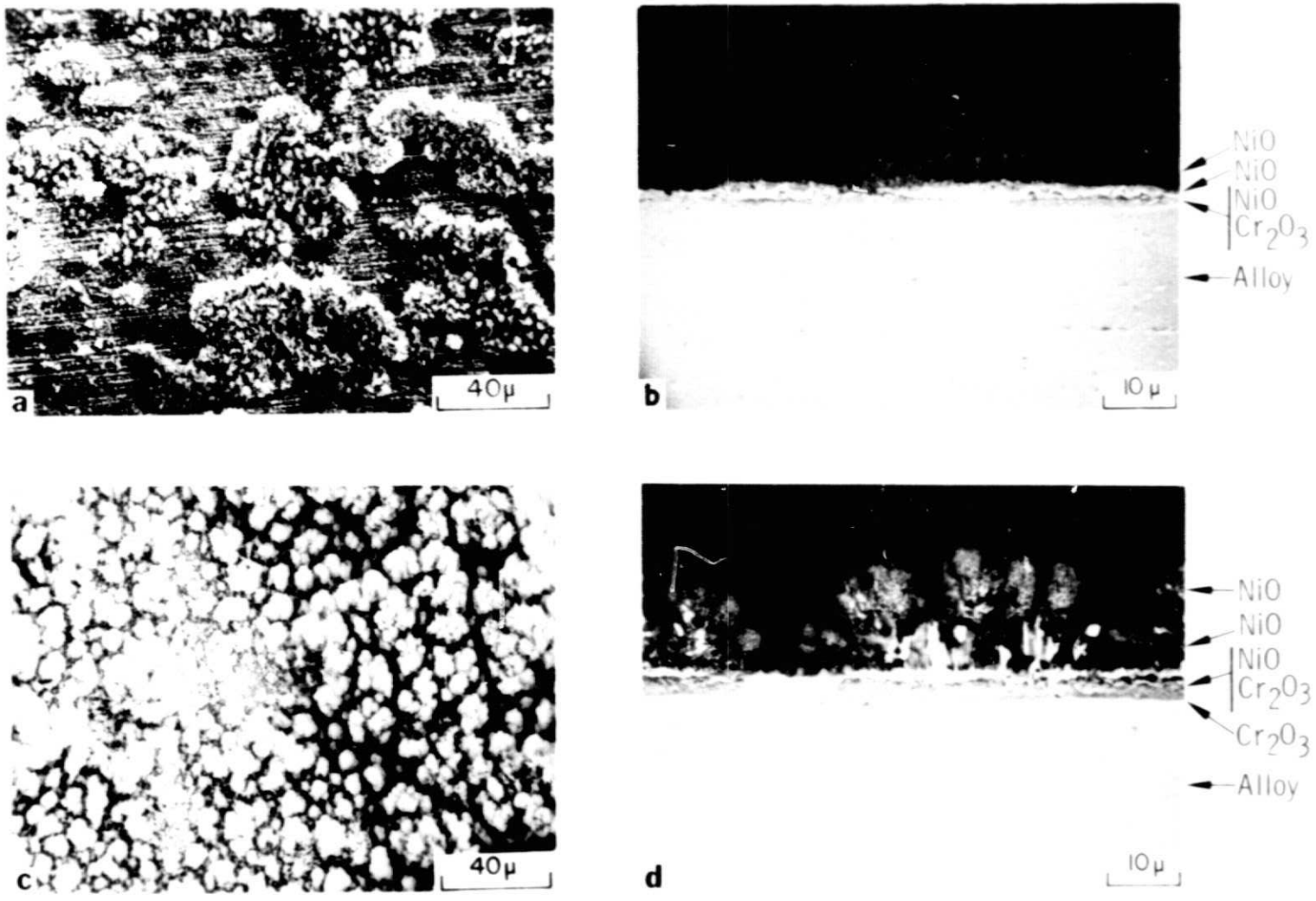

Figure 10. Oxide morphology and cross sections of mechanically polished specimens after (a), (b) 1 minute, and (c), (d) 10 minutes of dynamic oxidation.